Journal of Materials Chemistry B

Accepted Manuscript

ROYAL SOCIETY OF CHEMISTRY

www.rsc.org/materialsB

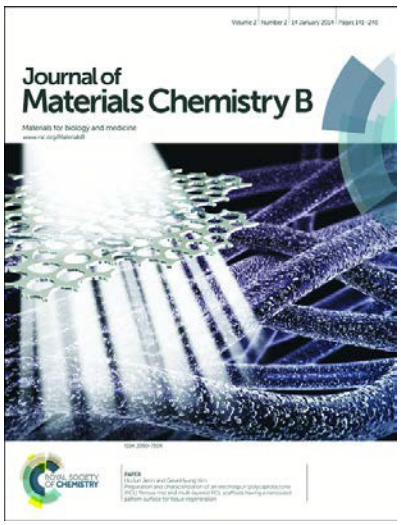

Journal of Materials Chemistry B

Materials for Biology and Medicine

Full paper submission

Journal of Materials Chemistry B is a weekly journal in the materials field. The journal is interdisciplinary, publishing work of international significance on all aspects of materials chemistry related to biology and medicine. Articles cover the fabrication, properties and applications of materials.

2013 Impact Factor of *Journal of Materials Chemistry*: **6.626**
For more information go to www.rsc.org/materialsB

The following paper has been submitted to *Journal of Materials Chemistry B* for consideration as a **full paper**.

Journal of Materials Chemistry B wishes to publish original research that demonstrates **novelty and advance**, either in the chemistry used to produce materials or in the properties/applications of the materials produced. Work submitted that is outside of these criteria will not usually be considered for publication. The materials should also be related to the theme of materials for biology and medicine.

Routine or incremental work, however competently researched and reported, should not be recommended for publication if it does not meet our expectations with regard to novelty and impact.

It is the responsibility of authors to provide fully convincing evidence for the homogeneity and identity of all compounds they claim as new. Evidence of both purity and identity is required to establish that the properties and constants reported are those of the compound with the new structure claimed.

Thank you for your effort in reviewing this submission. It is only through the continued service of referees that we can maintain both the high quality of the publication and the rapid response times to authors. We would greatly appreciate if you could review this paper in **two weeks**. Please let us know if that will not be possible.

Once again, we appreciate your time in serving as a reviewer. To acknowledge this, the Royal Society of Chemistry offers a **25% discount** on its books: http://www.rsc.org/Shop/books/discounts.asp. Please also consider submitting your next manuscript to *Journal of Materials Chemistry B*.

Best wishes,

FMcKenzie

Dr Fiona McKenzie
Executive Editor, *Journal of Materials Chemistry B*

Journal Name

ARTICLE

Controllable synthesis of polydopamine nanoparticles in microemulsions with pH-activatable properties for cancer detection and treatment

Received 00th January 20xx,
Accepted 00th January 20xx

DOI: 10.1039/x0xx00000x

www.rsc.org/

Fuyao Liu,[a,d] Xiuxia He,[c] Junping Zhang,[c] Hongda Chen,[a] Huimao Zhang*[,b] and Zhenxin Wang*[,a]

Polydopamine nanoparticles (PDA NPs) combining diagnostic and therapeutic functions are potentially useful in biomedicine. However, it is difficult to synthesize PDA NPs with relatively small size (≤50 nm in diameter) using traditional polymerization of dopamine monomers in alkaline water-ethanol solution at room temperature. Herein, PDA NPs with average diameters ranging from 25 nm to 43 nm are prepared in a way similar to the silica-like reverse microemulsion process. The size of PDA NPs can be modulated by changing the amount of dopamine monomers in the microemulsion. After conjugated with ferric ions (Fe^{3+}), the poly(ethylene glycol) modified Fe-PDA NPs(termed as PEG-Fe-PDA NPs) exhibit pH-activatable magnetic resonance imaging (MRI) contrast and high photothermal performance. The combinational small dimension and pH-activatable MRI contrast can greatly facilitate tumor accumulation and increase tumor imaging sensitivity against animal models *in vivo*. Completely inhibited tumor growth is achieved by the PEG-Fe-PDA NPs mediated photothermal therapy with MRI guided.

Introduction

The application of nanotechnology to medicine, also called nanomedicine, has already shown great potential in tumor treatment, which is poised to improve survival rate and life quality of patients through a more personalized medicine. During last two decades, various nanostructured materials including inorganic/organic nanoparticles (NPs) or nanorods (NRs), quantum dots (QDs), carbon nanotubes and two-dimensional nanosheets (*e.g.*, graphene) have been synthesized and employed to diagnose disease, improve treatment efficacy or combinations of these.[1-6] Very recently, polydopamine nanoparticles (PDA NPs), as a major pigment of naturally occurring melanin, have attracted widespread interest in theranostic field because of their excellent biocompatibility and reduced adverse effects caused by the administration of foreign substances.[7-12] For instance, Lu's group presented a novel photothermal therapeutic agent based on polydopamine colloidal nanospheres for *in vivo* cancer therapy.[7] An ideal theranostic nanoparticle requires not only to be safe and biodegradable, but also to have optimized diagnostic sensitivity and therapeutic efficiency. Among the physicochemical parameters of NPs, particle size is a critical characteristic to determine the biodistribution and tumor accumulation of the NPs *in vivo*, further providing important consideration for improved clinical effects.[13-16] The large NPs are rapidly taken up by the liver and spleen, resulting in few accumulation in tumors. The small NPs show reduced phagocytic capture of NPs by the cellular immune system, leading to long circulation and subsequent accumulation in tumor tissues attributed to the enhanced permeability and retention (EPR) effect.[15] However, controllable synthesis of PDA NPs of less than 50 nm in diameter is still a challenge.

The PDA NPs are normally synthesized by oxidative polymerization of dopamine (DA) monomers in the mixture of water, ethanol, and ammonia at room temperature.[7] The reaction mechanism is similar to the silica-like Stöber process, which is a pioneering method for synthesizing monodisperse silica NPs via the hydrolysis and condensation of silicon alkoxides in ethanol-water solution with ammonia as a catalyst.[17] However, it is difficult to obtain particle of sizes below 100 nm in diameter using the Stöber method.[18-19] In the late 1990s, the reverse microemulsion method was developed to produce monodisperse Si NPs with sizes ranging from 20 nm to 100 nm in diameter by Arriagada and Osseo-Asare.[20-21] This approach involves the ammonia-catalyzed polymerization of TEOS (tetraethoxysilane) in a water-in-oil microemulsion, which is a ideal strategy for producing monodisperse silica nanoparticles smaller than 100 nm.[18] Inspired by these research results, we wonder that the microemulsion strategy might be employed for the polymerization of DA, thereby

[a] State Key Laboratory of Electroanalytical Chemistry, Changchun Institute of Applied Chemistry, Chinese Academy of Sciences, Changchun, 130022, P. R. China.
[b] Department of Radiology, The First Hospital of Jilin University, Changchun, 130021, P. R. China.
[c] School of Life Science and Technology, Changchun University of Science and Technology, Changchun, 130022, P. R. China.
[d] University of Chinese Academy of Sciences, Beijing, 100039, P. R. China.
E-mail: huimaozhanglinda@163.com (HZ) and wangzx@ciac.ac.cn (ZW).

† Electronic Supplementary Information (ESI) available: Seventeen supplementary figures and two supplementary tables. See DOI: 10.1039/x0xx00000x

generating PDA NPs with highly monodisperse and relatively small size.

For obtaining high quality imaging results, the sensitivity of imaging agents/probes should be a top consideration, which strongly depends on target-to-background ratio. However, the signals of the most of imaging agents/probes are "always on" regardless of their proximity to and/or interaction with the tumors, resulting in the poor target-to-background ratio. The phenomenon makes the tissue of interest more difficult to highlight.[22-23] Development of an activatable imaging agents in response to specific biological stimuli would help to maximize the signal from the target and minimize background signal, showing obvious advantages.[24-29] Consequently, introducing stimuli-tunable small PDA NPs with theranostic functionalities would be of great value, as it provides more flexibility for multiplexing in biomedical applications including diagnosis and therapy.

Herein, we demonstrate a simple reverse microemulsion-based method to elaborate pH-activatable poly(ethylene glycol) modified Fe-PDA NPs (termed as PEG-Fe-PDA NPs) for magnetic resonance imaging (MRI) guided photothermal therapy (PTT) for the first time. The synthesis of PEG-Fe-PDA NPs is highly simple and controllable without using any special equipment. By varying the reaction conditions, we found that the average sizes of PDA NPs can be precisely tuned from 25 nm to 43 nm in diameter. The PEG-Fe-PDA NPs are easily obtained by successively incubating the as-prepared PDA NPs with Fe^{3+} and PEG in aqueous solution at room temperature. The nonionic PEG coating not only improve the stability of NPs in different dispersing media, but also provide a passivated NP surface. The absorption of PDA extends to NIR region, which have made PEG-Fe-PDA NPs a novel photothermal agent. In addition, the functionalized paramagnetic Fe^{3+} ions on PEG-Fe-PDA NPs, contribute to the significant enhancement in MRI. Above all, the PEG-Fe-PDA NPs with small size indicate acid-enhanced magnetic resonance contrast, high photothermal efficiency and preferential accumulation in tumors, which is ideal for sensitive MRI tumor imaging and efficient photothermal therapy (PTT) of tumor. These results highlighted new directions in the design of a smart theranostic nanostructure that could be utilized for the clinical application.

Experimental

Materials.

Polyoxyethylene (5) nonylphenyl ether (Igepal CO-520.Mn=441) and Leibovitz's L-15 medium (L-15) were obtained from Sigma-Aldrich Co. (St Louis, USA). Dopamine hydrochloride (DA·HCl, 99%), ammonium hydroxide (ACS, 28.0-30.0% NH_3 by weight) and iron(III) chloride hexahydrate ($FeCl_3 \cdot 6H_2O$) were obtained from Alfa Aesar. (Ward Hill, USA). Methoxy polyethylene glycol thiol (mPEG-SH, M.W. 2000) was purchased from Yarebio. Co. Ltd. (Shanghai, China). Fetal bovine serum (FBS) was obtained from Gibco. (New York, USA). 3-(4,5-dimethylthiazol-2-yl)-2,5-diphenyltetrazolium bromide (MTT) was received from Beijing Dingguo Biotechnology Ltd. (Beijing, China). Other reagents (analytical grade) were purchased from Beijing Chemical Reagents Company (Beijing, China). All reagents were used without further purification. Milli-Q water (18.2 MΩ cm) was used in all experiments.

Characterizations.

Transmission electron microscope (TEM) micrographs were recorded by a Hitachi H-600 electron microscope with an acceleration voltage of 100 kV (Hitachi Ltd., Tokyo, Japan). X-ray diffraction analysis (XRD) were carried out on a D8 ADVANCE diffractometer (Bruker Co., Germany) using Cu Kα (0.15406 nm) radiation. X-ray photoelectron spectroscopy (XPS) measurements were conducted with a VG ESCALAB MKII spectrometer (VG Scientific Ltd., UK). The infrared spectra were conducted with a Bruker Vertex 70 Fourier transform infrared spectrometer (FT-IR). DLS and Zeta potential of the as-prepared samples were determined using a Zetasizer Nano ZS (Malvern Instruments Ltd., UK). The analysis of elements were determined by a ELAN 9000/DRC ICP-MS system (Perkin Elmer, USA).

Synthesis of PEG-Fe-PDA NPs.

Ammonium hydroxide (80 μL, 28 wt% in water) was added into the mixture containing cyclohexane (10 mL) and Igepal CO-520 (0.65 mL) followed by ultrasonic treatment for 20 min. After stirred for another 30 min, DA·HCl aqueous solutions (25 wt%) with various volumes (7.5μL to 120 μL) were injected into the above reaction mixture, respectively. After stirred for 24 h at 20 °C, the NPs were precipitated by adding ethanol, collected by centrifugation (10000 rpm for 10 min) and washed with 30 mL ethanol (two times) and 30 mL water (two times). Finally, the polydopamine nanoparticles (PDA NPs) were redispersed in water and dried by vacuum evaporation. To examine the effects of synthetic parameters, the amount of ammonium hydroxide and the reaction temperature were varied systematically. From the standard synthetic conditions described above, the amount of ammonium hydroxide ranged from 40 to 160 μL and reaction temperature ranged from 10 to 50 °C.

The PDA NPs (10 mL, 1 mg/mL) were then incubated with Fe^{3+} solution (500 μL, 1 mg/mL) under vigorous stirring. After 3 h, Fe^{3+}-bound PDA NPs (Fe-PDA NPs) were retrieved by centrifugation (14000 rpm) and washed with 30 mL water (three times). Finally, the as-prepared Fe-PDA NPs (100 mg) were reacted with mPEG-SH (300 mg) in TB (Tris buffer, pH 8.5) under vigorous stirring for 12 h. PEGylated Fe^{3+}-PDA NPs (PEG-Fe-PDA NPs) were purified by centrifugation (10000 rpm, three times), and redispersed in water. The Fe^{3+} amounts of PEG-Fe-PDA NPs were measured by inductively coupled plasma-mass spectrometry (ICP-MS) analysis. PEG-Fe-PDA NPs (100 nm in diameter) were prepared according to previous literature.[11]

Measurement of Photothermal performance.

The aqueous solution of PEG-Fe-PDA NPs with different concentrations (0, 31.25, 62.5, 125, and 250 ppm) were irradiated by an 808 nm NIR laser at a power density of 1.3 W cm^{-2} for 10 min, respectively. The temperature elevation of solution was recorded as a function of time by a thermometer

with a thermocouple probe. Pure water was used as a negative control.

Cell Viability Assay and Cell uptake.

The SW620 human colon cancer cells and osteoblastic MC3T3-E1 cells were obtained from Shanghai Cell Bank, Chinese Academy of Sciences. To quantitatively evaluate the photothermal efficacy of NPs, SW620 cells were incubated with desired amounts of PEG-Fe-PDA NPs, and then irradiated by an 808 nm NIR laser (1.3 W cm^{-2}) for 6 min, respectively. After irradiation, the culture media were replaced with fresh L-15 and incubated for another 24 h. Finally, the cell viabilities were evaluated by a standard MTT assay.[30] The untreated SW620 cells were used as control sample. The relative cell viabilities (%) were calculated by using the optical densities with respect to the control value. The cell viabilities (%) of the PEG-Fe-PDA NPs stained cells were also measured by MTT assay under an identical experimental set up except 808 nm NIR laser irradiation. For live/dead cell staining experiment, the cells were seeded in 96-well plates. After incubated with PEG-Fe-PDA NPs and irradiated by an 808 nm NIR laser (1.3 W cm^{-2}) for 6 min, the cells were stained with both calcein AM and PI, and imaged by a confocal fluorescence microscopy (Leica, CLSM TCS-SP2, Wetzlar, Germany), respectively. For comparison, the relative cell viabilities (%) of PEG-Fe-PDA NPs stained MC3T3-E1 cells were also measured by the MTT assay.

For *In vitro* MR imaging, the cells were incubated in 2 mL fresh L-15 containing various amounts of PEG-Fe-PDA NPs and incubated for 12h in a humidified 5% CO_2 atmosphere at 37 °C. Subsequently, the cells were washed three times with PBS, detached by 1 mL trypsin/EDTA cell detaching kit (Gibco). After centrifugation at 2000 rpm for 5 min, the supernatants were discharged. Finally, the MR imaging of cell pellets were performed using a Siemens 1.5 T MRI scanner (Magnetom Avanto, Siemens, Erlangen, Germany).

In vivo MRI imaging and photothermal therapy.

Nude mice with average weight of 20 g were purchased from Vital River Company (Beijing, China). Animal procedures complied with the guidelines of the Regional Ethics Committee for Animal Experiments established by Jilin University Institutional Animal Care and Use. The tumor models were prepared by implanting 5×10^6 SW620 cells suspended in 100 μL of serum free L-15 in the nude mice subcutaneously.

To investigate the pH-activatable MRI performance of PEG-Fe-PDA NPs in tumor, nude mice were anesthetized using chloral hydrate (10 wt%). PEG-Fe-PDA NPs suspended in 100 μL NaCl solutions (0.9 wt%) were injected intratumorly into the mouse at a dose of 0.25 mg Fe kg^{-1} (body weight). MRI imaging was performed using a Siemens 1.5 T MRI scanner (Magnetom Avanto, Siemens, Erlangen, Germany) before and after injection at desired time points. Imaging parameters were as follows: TR, 358 ms; TE, 15 ms; field of view, 120 mm × 72 mm and slice thickness, 2.0 mm, respectively. For *in vivo* tumor accumulation study, 80 μL 0.5 mg mL^{-1} Fe of the PEG-Fe-PDA NPs (25 nm and 100 nm) were injected intravenously into the mouse instead.

For photothermal therapy, when the tumor size reached about 5 mm in diameter, the nude mice were anaesthetized and intravenously injected with PEG-Fe-PDA NPs suspended in NaCl solutions (100 μL, 2 mg mL^{-1}). After 1.5 h injection, the tumors were irradiated by an 808 nm laser at 1.3 W cm^{-2} for 6 min. The tumor dimensions were measured using a caliper every other day after the treatment for 20 days. The tumor volumes were calculated according to the following equation: Tumor volume = (tumor length) × (tumor width)^2/2. The relative tumor volumes were calculated as V/V_0 (V_0 was the tumor volume before PEG-Fe-PDA NPs administration and laser irradiation).

Evaluating the biocompatibility of PEG-Fe-PDA NPs.

For *in vivo* toxicity studies, PEG-Fe-PDA NPs suspended in NaCl solutions (0.9 wt%) at a dose of 10 mg kg^{-1} was administrated intravenously into healthy mice. The mice were weighted every day over one month period. Then, the mice were sacrificed and the tissues including heart, spleen, liver, lung, and kidney were fixed in 10% neutral buffered formalin. The histological sections were stained with hematoxylin-eosin (HE) for histopathological analysis under the optical microscope observation. The blood were collected for hematology analysis and blood biochemistry assay.

Results and discussion

Synthesis and characterization of PEG-Fe-PDA NPs.

We developed a simple reverse microemulsion-based method for preparing monodisperse PDA NPs with controllable morphology and size. Fig. 1a and S1† illustrates the detailed reaction process of the strategy. Reverse microemulsions are highly isotropic and thermodynamically stable systems that consist of a homogeneous mixture of ammonia water, oil (cyclohexane), and surfactant molecules (Igepal CO-520). The ammonia water droplets are dispersed as nanosized liquid entities in the bulk oil phase, which then act as a confined nanoreactor for the synthesis of these NPs.[20] In the presence of oxidant (*i.e.*, oxygen), the monomer, DA, can be oxidized and spontaneously self-polymerize under alkaline conditions (pH > 7.5).[9] When an DA solution is added into microemulsion, the diffusion of DA into the ammonia water droplets form PDA NPs through self-polymerization, resulting in the color of mixture changes from colorless to pale brown, and finally turning to deep brown with passing time. The nucleation and growth kinetics of the DA are highly regulated in the ammonia water droplets of the microemulsion system, leading to the formation of highly monodisperse PDA NPs under very mild reaction conditions without the requirement of any complicated instrumentation. In particular, the size and shape of PDA NPs can be simply controlled by varying microemulsion/reaction parameters (as shown in Fig. 1b and S2-S5†).For instance, the average sizes of synthetic PDA NPs can be precisely controlled from 25 nm to 43 nm by increasing the amount of DA monomer in the reaction mixture (as shown in Fig. 1b, S2†, S3b† and S4†) under the optimum condition (80

Journal Name

ARTICLE

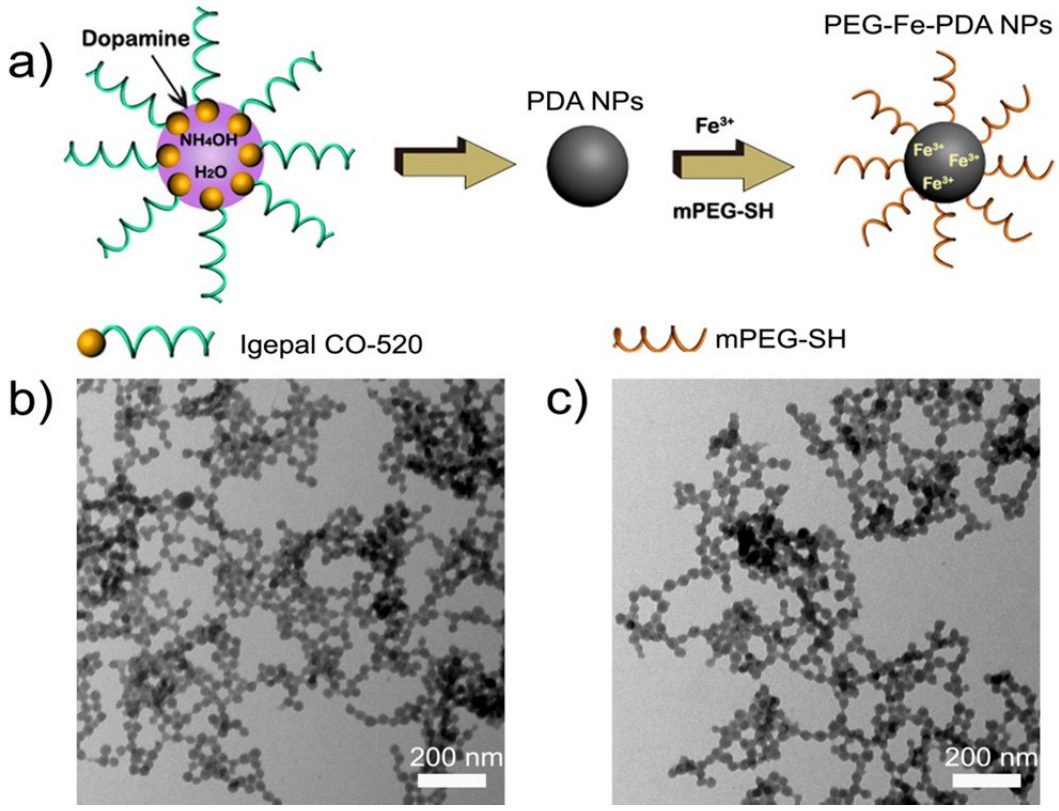

Fig. 1. (a) Schematic illustration of the synthesizing process of PEG-Fe-PDA NPs, the illustration is not drawn to scale. (b) TEM micrograph of PDA NPs (25 ± 2.0 nm in diameter, obtained with 7.5 µL of dopamine hydrochloride aqueous solution). (c) TEM micrograph of PEG-Fe-PDA NPs.

µL of ammonium hydroxide and 20 ° C reaction temperature).The X-ray diffraction data indicates that the as-prepared PDA NPs are amorphous materials (as shown in Fig. S6†). The 25 nm PDA NPs were typically used for exploring the capacity of the as-prepared PDA NPs in further experiments, because the NPs with small size can not only remain in the circulation for an extended period of time, but also easily pass through small pores in the blood vessel wall and efficiently accumulate in tumor tissues through EPR effect.[15] To investigate the possibility of PDA NPs as a platform for magnetic resonance imaging (MRI), the as-prepared PDA NPs were treated with Fe^{3+} solution to prepare Fe^{3+}-bound PDA NPs (named as Fe-PDA NPs). The formation of Fe-PDA NPs was confirmed by energy-dispersive X-ray spectroscopy (EDS) (as shown in Fig. S7 †) and X-ray photoelectron spectroscopy (XPS) (as shown in Fig. S8†). The Fe-PDA NPs were further functionalized with thiol-terminated methoxy-poly(ethylene glycol) (mPEG-SH) through the Michael addition reaction, which is believed to involve reaction between terminal thiol groups and the catechol/quinine groups of PDA (as shown in Fig. S1†). The surface immobilized PEG can improve the stability of NPs in physiological conditions and favor the accumulation of NPs in tumor by the EPR effect.[8,31] The presence of PEG on NP surface was confirmed by the absorption bands at 2928 cm^{-1} (alkyl C-H stretching) and 1088 cm^{-1} (C-O-C stretching) in the FT-IR spectrum of PEG-Fe-PDA NPs (as shown in Fig. S9†).[8] The hydrodynamic diameter and zeta potential of PEG-Fe-PDA NPs are 48 nm±1.3 nm (PDI: 0.18) and -8.79 mV, respectively (as shown in Fig. S3a† and S10†). In addition, the PEG-Fe-PDA NPs exhibit excellent stability in different dispersants including H_2O, PBS, TB, 0.9% NaCl solution and DMEM supplemented with 10% FBS (as shown in Fig. S11†). The stability of conjugated between Fe^{3+} and catechol ligand of PDA NPs was also confirmed by the EDS characterization (as shown in Fig. S12†). The amount of Fe^{3+} in PEG-Fe-PDA NPs was measured as 11.2 µg of Fe per mg of NPs using ICP-MS.

MRI of PEG-Fe-PDANPs.

Journal Name

ARTICLE

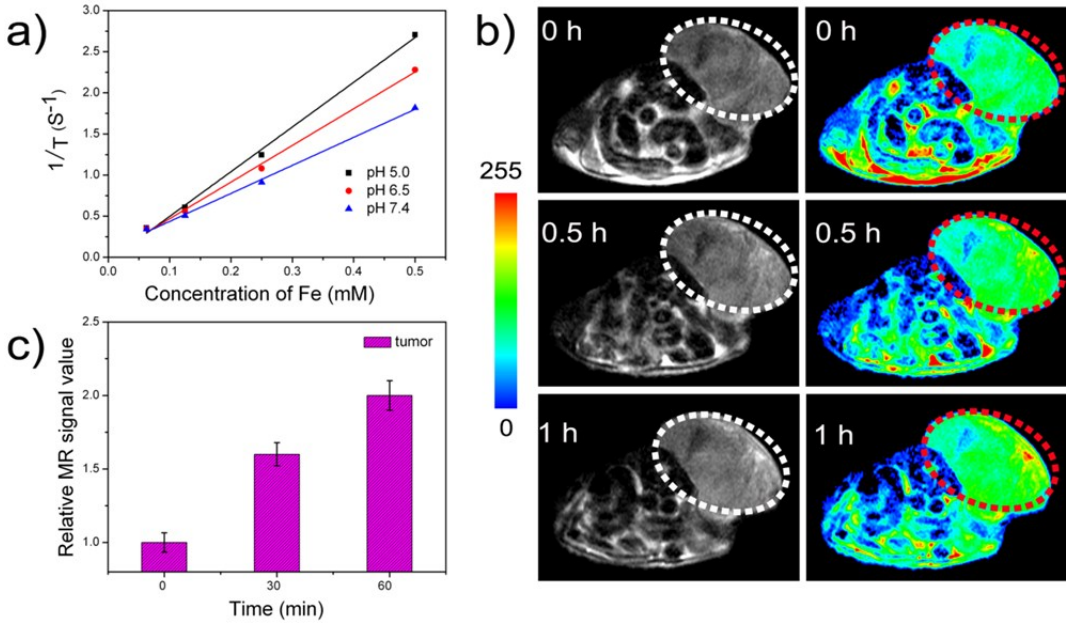

Fig. 2. (a) R1 relaxivity of PEG-Fe-PDA NPs as a function of the molar concentration of Fe^{3+} in the solution under different pH values. (b) *In vivo* transversal cross-sectional MR images of nude mice bearing colorectal tumor (SW620) after intratumor injection (tumor, ellipses) of PEG-Fe-PDA NPs at different time intervals (The time 0 h means pre-injection.). (c) Corresponding data analysis of tumor in (b). Error bars mean standard deviations (n=5).

Previous studies have demonstrated that coordination between Fe^{3+} and catechol ligand of PDA NPs is pH dependent.[32-35] The reduced coordination number in mild acid condition can enhance the quantity and mobility of the coordinated water in the first and second coordination spheres around Fe paramagnetic center, which further improve the relaxivity.[36-39] To examine its pH-responsive MRI contrast properties, the longitudinal relaxivity ($r1$) of PEG-Fe-PDA NPs was measured under various pH values. The $r1$ value is significantly increased from 3.4 mM^{-1} s^{-1} to 4.5 mM^{-1} s^{-1} and finally to 5.4 mM^{-1} s^{-1} when solution pH is decreased from 7.5 to 5.0 (as shown in Fig. 2a). The increasing $r1$ can be attributed to transitions between mono- and bis-complex states. Such a pH-activatable MRI performance is very beneficial to the tumor detection because the acidic nature of tumor tissues can help to improve the MRI contrast efficiency of PEG-Fe-PDA NPs, while the normal tissues with neutral essence do not show such an effect.[36]

For evaluating their MRI imaging capability, *in vitro* T1-weighted MR images of the PEG-Fe-PDA NPs stained SW620 cells were examined on a Siemens 1.5 T MRI scanner. The signal intensity is increased significantly with increasing the concentration of PEG-Fe-PDA NPs, which firmly supported the labeling capability of PEG-Fe-PDA NPs and demonstrated its potential application as molecular MRI probes (as shown in Fig. S13†).[40-41] Similarily, the signal intensity is increased significantly with increasing the incubation time with PEG-Fe-PDA NPs (as shown in Fig. S13†). Importantly, PEG-Fe-PDA NPs provide an excellent platform for pH-activatable enhancement of MRI contrast due to the special interaction between Fe^{3+} and catechol ligand. The signal amplifying property makes PEG-Fe-PDA NPs an ideal probe for tumor imaging. A nude mouse-bearing colorectal tumor (SW620) was established for evaluating the pH-activatable enhancement of MRI contrast of PEG-Fe-PDA NPs *in vivo*. Accompanying the acid induced catechol-Fe complexs transition, a time course of signal enhancement was clearly observed in T1-weighted imaging of the tumor when PEG-Fe-PDA NPs was intratumorly administrated to a mouse (as shown in Fig. 2b and 2c). The signal enhancement area also gradually expanded after the intratumor injection (as shown in Fig. 2b), which was attributed to the diffusion process of PEG-Fe-PDA NPs. This inspiring phenomenon gave the first evidence on that the pH-activatable PEG-Fe-PDA NPs could be utilized for sensitive and tumor-specific MRI.

Building on these results, we established a T1-weighted MRI on subcutaneous SW620 cancer model to evaluate its potential preferential tumor accumulation. After intravenous injection of PEG-Fe-PDA NPs, wholebody imaging was performed at different time points of post injection with a

Siemens 1.5 T MRI scanner. A sustained increase of T1 contrast in the tumor over time was observed from 0 to 1.5 h after particle injection, indicating the effective uptake of PEG-Fe-PDA NPs in the tumor by the EPR effect (as shown in Fig. 3a). The MRI signal of tumor reaches a maximum value at 1.5 h post injection. The MRI effectively delineates the proximal edge of the tumor at this time point (as shown in Fig. 3a). Contrarily, low contrast change in the normal tissue was observed through the same period (as shown in Fig. 3). The

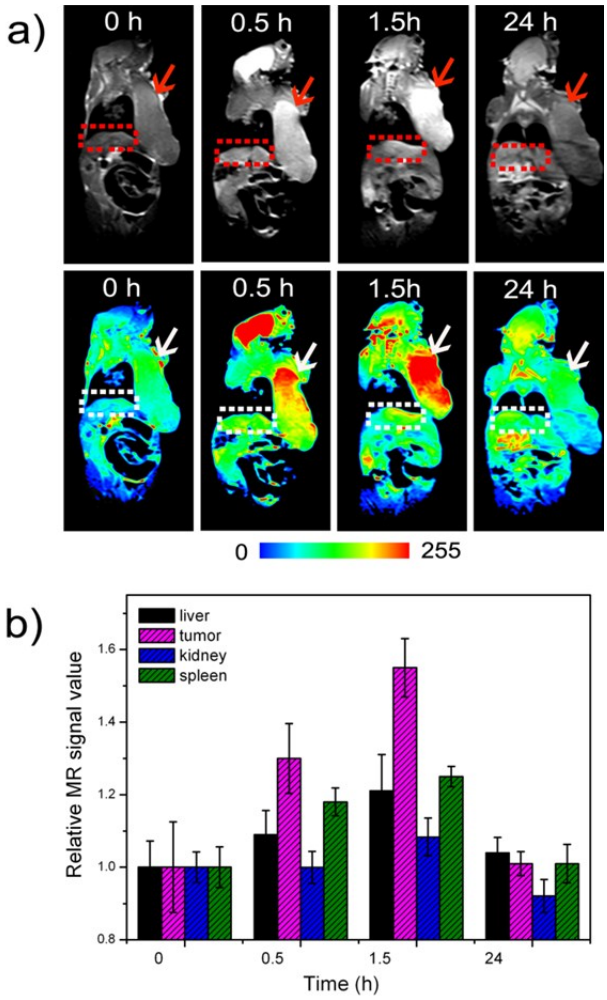

Fig. 3. (a) *In vivo* MR images of nude mice bearing colo-rectal tumor after intravenous injection (tumor, arrows; liver, rectangles) of PEG-Fe-PDA NPs at different time intervals (The time 0 h means pre-injection.). (b) Corresponding data analysis of tumor, liver, kidney and spleen in (a). Error bars mean standard deviations (n=5).

result confirms that the MRI signal enhancement in the liver and spleen (the main RES organ) is lower than that of tumor site. When the PEG-Fe-PDA NPs are circulating in blood, the PEG-Fe-PDA NPs can be accumulated in tumor siteand gradually dissociated under acidic environments, resulting in Fe-catechol complexes transitions from bis-coordination to mono-coordination.[32] Due to the reduction of coordination number, Fe paramagnetic centers become more accessible to water molecules. These phenomena result in the stronger MRI contrast at the tumor site than the liver.[36] For comparison, the MR images of mice injected with large NPs (~100 nm, as shown in Fig. S14†) was performed at the same time points. The large NPs are rapidly taken up by the liver and spleen, resulting in less accumulation in tumor (as shown in Fig. S15†). The above results also demonstrated that the small PEG-Fe-PDA NPs could be used to the detection of tumor microenvironment, for instance, discrimination of pH variation at tumor site.

PTT of PEG-Fe-PDA NPs.

PEG-Fe-PDA NPs with strong absorbance in the NIR band motivates us to investigate their potential as a photothermal agent (as shown in Fig. S16†).[42] Fig. 4a shows the heating curve of PEG-Fe-PDA NPs solution with different concentrations using an 808 nm diode laser at 1.3 W cm^{-2}. An obvious concentration-dependent temperature increase is observed in Fig. 4a. The solution temperature can be rapidly increased to 50 °C (the temperature of efficient killing of cancerous cells[43]) when the concentration of PEG-Fe-PDA NPs is 250 μg mL^{-1}. The solution temperature can be eventually leveled off during 8 min when the NIR irradiation is stopped. The rapid cooling of the solution suggests a good thermal conductivity of PEG-Fe-PDA NPs. Furthermore, the negligible absorption change is observed when PEG-Fe-PDA NPs has been irradiated for over 60 min, indicating that the PEG-Fe-PDA NPs has good photothermal stability (as shown in Fig. S17†). SW620 cells were then utilized for evaluating the possible cytotoxicity and PTT efficacy of PEG-Fe-PDA NPs *in vitro*. The PEG-Fe-PDA NPs alone show little cytotoxicity at a wide range of concentrations, indicating their low cytotoxicity and high biocompatibility (as shown in Fig. S18†). In the presence of 250 μg mL^{-1} PEG-Fe-PDA NPs in the culture medium, more than 80% of cells were killed after irradiating under 808 nm NIR laser for 6 min (as shown in Fig. 4b). To further identify the PTT efficacy of PEG-Fe-PDA NPs *in vitro*, PEG-Fe-PDA NPs treated SW620 cells with or without 808 nm NIR laser irradiation were co-stained by Calcine AM and propidium iodide (PI) and imaged by confocal microscopy, respectively (as shown in Fig. 4c). The confocal microscopic result is consistent with that of MTT assay. The experimental result indicates that PEG-Fe-PDA NPs can be used as efficient PTT agents.

On the basis of high PTT efficiency *in vitro* and efficient passive targeting in tumor, we proceeded to evaluate the therapeutic potential of PEG-Fe-PDA NPs in xenograft tumor mouse models. For the PTT group, mice were intravenously injected with PEG-Fe-PDA NPs. The tumor site was then irradiated by 808 nm NIR laser (1.3 W cm^{-2}) for 6 min at 1.5 h post-injection. Comparison with the control group and the group with NPs injected but no irradiation, PEG-Fe-PDA NPs-mediated PTT exhibits significant delay in tumor growth (as shown in Fig. 5a and 5b). Histological examination confirmed that PEG-Fe-PDA NPs-mediated PTT caused substantial damage to the tumor (as shown in Fig. S19†). In this group of mice, the most of tumor tissue was necrotized. Conversely, in the control animals and mice treated with PEG-Fe-PDA NPs only, there was negligible necrosis in tumor tissue. The PTT

Journal Name

ARTICLE

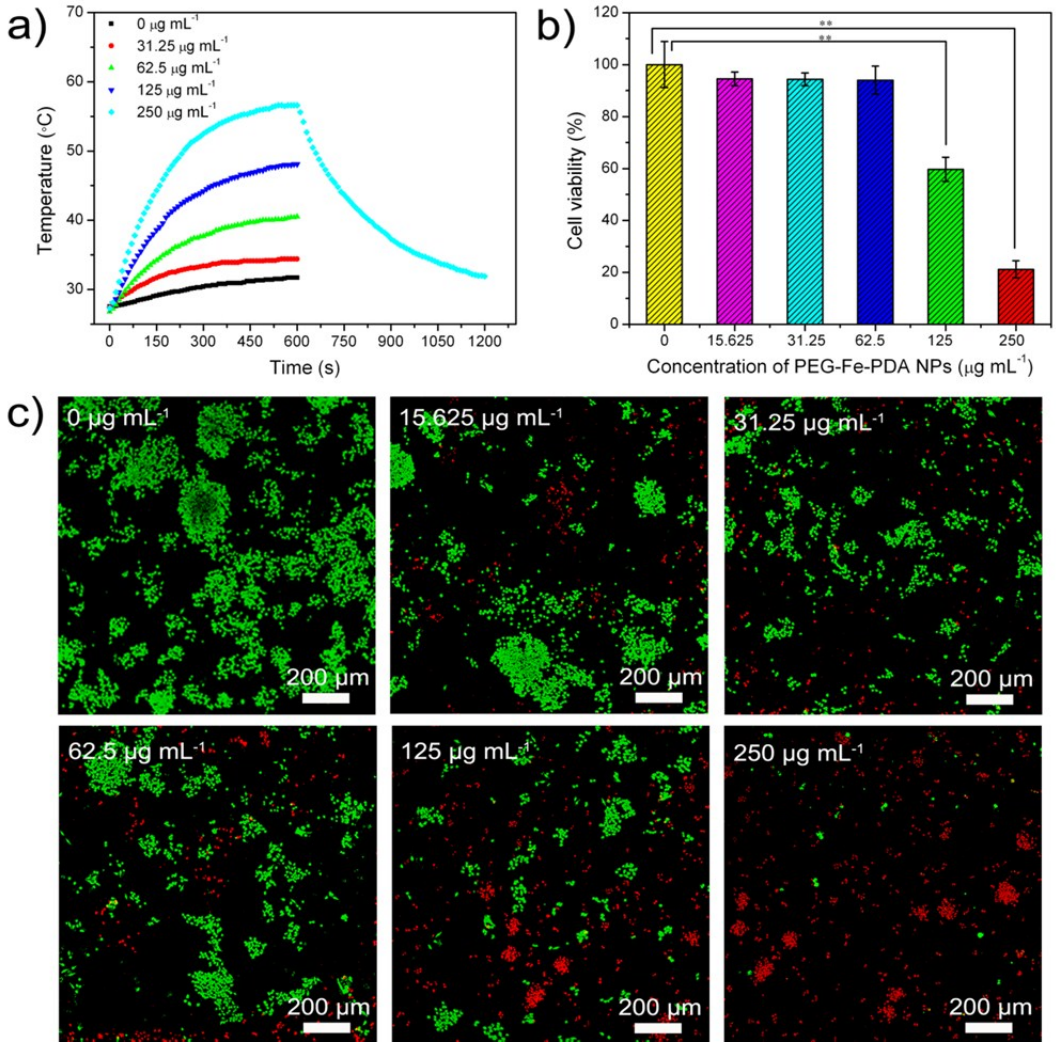

Fig. 4. (a) Temperature elevation of water and PEG-Fe-PDA NPs solutions with various concentrations (0-250 μg mL^{-1}) over a period of 10 min under exposure of 808 nm NIR light (1.3 W cm^{-2}). The temperatures were measured every 10 s using a ther-mometer. (b) In vitro cell viabilities of SW620 cells incubated with various concentrations of PEG-Fe-PDA NPs (0-250 μg mL^{-1}) with 808 nm NIR laser irradiation (1.3 W cm^{-2}, 6 min). The error bars mean standard deviations (n=5, **p < 0.01, by ANOVA with Tukey's post-test). (c) Confocal fluorescence images of SW620 cells after incubation with various concentrations of PEG-Fe-PDA NPs (0-250 μg mL^{-1}) with 808 nm NIR laser irradiation for 6 min. The cells were co-stained with calcine AM (green, living cells) and PI (red, dead cells).

result indicates that PEG-Fe-PDA NPs are capable of imaging guided tumor therapy in vivo.

In vivo toxicology investigation.

Furthermore, the long-term *in vivo* toxicity of PEG-Fe-PDA NPs was examined by histochemical analysis, hematology analysis and blood biochemical assays. Neither death nor significant body weight drop was noted in all test groups (as shown in Fig. S20†). And there are no distinct toxicity of the PEG-Fe-PDA NPs to various organs relative to the controls (as shown in Fig. 5c and 5d). For hematology analysis and blood biochemical assays, there is negligible difference between treated group and control group after one month post-injection of PEG-Fe-PDA NPs (as shown in Table S1), which further confirms the non-toxicity of PEG-Fe-PDA NPs. Although the *in vivo* toxicity results shown here are preliminary, the PEG-Fe-PDA NPspresent great promise as non-toxic pH-activatable theranostic nanoplatform for applications in biological medicine.

Journal Name

ARTICLE

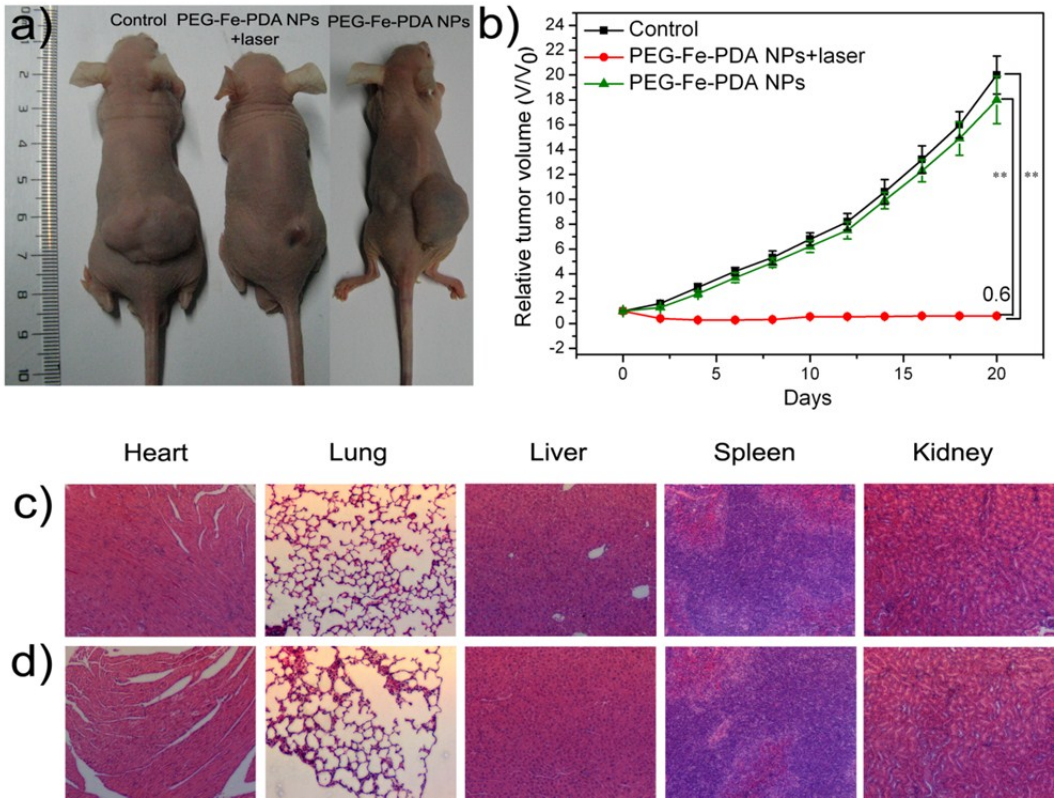

Fig. 5. (a) Digital photographs of the mice which were collected from different groups at the end of intravenous treatments (day 20). (b) Corresponding tumor growth curves of different groups of mice after intravenous treatments. Error bars mean standard deviations (n=5, **p < 0.01, by ANOVA with Tukey's post-test). Histological changes of (c) healthy mouse without injection of PEG-Fe-PDA NPs and (d) the mouse after 30 days post-injection of a single dose of PEG-Fe-PDA NPs, respectively.

Conclusions

In summary, we have demonstrated the use of reverse microemulsion method to prepare pH-activatable PEG-Fe-PDA NPs integrating diagnostic and therapeutic functions through the self-polymerization reaction of dopamine. The as-prepared PDA NPs are highly monodisperse and controllable with the average sizes ranging from 25 nm to 43 nm in diameter. Using 25 nm PDA NPs as a typical example, the PEG-Fe-PDA NPs exhibit pH-activatable MRI contrast, high photothermal efficiency and excellent biocompatibility. Sensitive MRI and efficiently PTT of tumor has been demonstrated in both cellular level in vitro and tumor-bearing small animal in vivo. The complementary experimental results indicate that PEG-Fe-PDA NPs show great promise as a theranostic agent for clinical translation.

Acknowledgements

The authors thank National Basic Research Program of China (No. 2011CB935800) for financial support.

Notes and references

1 T. Lammers, S. Aime, W. E. Hennink, G. Storm and F. Kiessling, *Accounts of Chemical Research*, 2011, **44**, 1029-1038.
2 N. S. Karan, A. M. Keller, S. Sampat, O. Roslyak, A. Arefin, C. J. Hanson, J. L. Casson, A. Desireddy, Y. Ghosh, A. Piryatinski, R. Iyer, H. Htoon, A. V. Malko and J. A. Hollingsworth, *Chemical Science*, 2015, **6**, 2224-2236.
3 J. Shi, Z. Xiao, N. Kamaly and O. C. Farokhzad, *Accounts of Chemical Research*, 2011, **44**, 1123-1134.
4 M. J. Sailor and J.-H. Park, *Advanced Materials*, 2012, **24**, 3779-3802.
5 Z. Fan, X. Huang, C. Tan and H. Zhang, *Chemical Science*, 2015, **6**, 95-111.
6 D.-E. Lee, H. Koo, I.-C. Sun, J. H. Ryu, K. Kim and I. C. Kwon, *Chemical Society Reviews*, 2012, **41**, 2656-2672.
7 Y. Liu, K. Ai, J. Liu, M. Deng, Y. He and L. Lu, *Advanced Materials*, 2013, **25**, 1353-1359.

8 F. Liu, X. He, Z. Lei, L. Liu, J. Zhang, H. You, H. Zhang and Z. Wang, *Advanced Healthcare Materials*, 2015, **4**, 559-568.
9 Y. Liu, K. Ai and L. Lu, *Chemical Reviews*, 2014, **114**, 5057-5115.
10 K.-Y. Ju, S. Lee, J. Pyo, J. Choo and J.-K. Lee, *Small*, 2015, **11**, 84-89.
11 K.-Y. Ju, J. W. Lee, G. H. Im, S. Lee, J. Pyo, S. B. Park, J. H. Lee and J.-K. Lee, *Biomacromolecules*, 2013, **14**, 3491-3497.
12 A. Postma, Y. Yan, Y. Wang, A. N. Zelikin, E. Tjipto and F. Caruso, *Chemistry of Materials*, 2009, **21**, 3042-3044.
13 S. Zhang, J. Li, G. Lykotrafitis, G. Bao and S. Suresh, *Advanced Materials*, 2009, **21**, 419-424.
14 H. Gao, W. Shi and L. B. Freund, Proceedings of the National Academy of Sciences of the United States of America, 2005, **102**, 9469-9474.
15 G. Zhang, Z. Yang, W. Lu, R. Zhang, Q. Huang, M. Tian, L. Li, D. Liang and C. Li, *Biomaterials*, 2009, **30**, 1928-1936.
16 K. Miki, H. Hashimoto, T. Inoue, H. Matsuoka, H. Harada, M. Hiraoka and K. Ohe, *Small*, 2014, **10**, 3119-3130.
17 W. Stöber, A. Fink and E. Bohn, *Journal of Colloid and Interface Science*, 1968, **26**, 62-69.
18 J. L. Vivero-Escoto, R. C. Huxford-Phillips and W. Lin, *Chemical Society Reviews*, 2012, **41**, 2673-2685.
19 R. P. Bagwe, C. Yang, L. R. Hilliard and W. Tan, *Langmuir*, 2004, **20**, 8336-8342.
20 F. J. Arriagada and K. Osseo-Asare, *Journal of Colloid and Interface Science*, 1999, **211**, 210-220.
21 K. D. Hartlen, A. P. T. Athanasopoulos and V. Kitaev, *Langmuir*, 2008, **24**, 1714-1720.
22 H. Kobayashi and P. L. Choyke, *Accounts of Chemical Research*, 2010, **44**, 83-90.
23 M. L. Viger, J. Sankaranarayanan, C. de Gracia Lux, M. Chan and A. Almutairi, *Journal of the American Chemical Society*, 2013, **135**, 7847-7850.
24 Y. Wang, K. Zhou, G. Huang, C. Hensley, X. Huang, X. Ma, T. Zhao, B. D. Sumer, R. J. DeBerardinis and J. Gao, *Nat Mater*, 2014, **13**, 204-212.
25 P. Shi, Z. Liu, K. Dong, E. Ju, J. Ren, Y. Du, Z. Li and X. Qu, *Advanced Materials*, 2014, **26**, 6635-6641.
26 Z. Zhao, H. Fan, G. Zhou, H. Bai, H. Liang, R. Wang, X. Zhang and W. Tan, *Journal of the American Chemical Society*, 2014, **136**, 11220-11223.
27 D. Ye, A. J. Shuhendler, P. Pandit, K. D. Brewer, S. S. Tee, L. Cui, G. Tikhomirov, B. Rutt and J. Rao, *Chemical Science*, 2014, **5**, 3845-3852.
28 C. Tu, R. Nagao and A. Y. Louie, *Angewandte Chemie*, 2009, **121**, 6669-6673.
29 Z. Li, Y. Song, Y. Yang, L. Yang, X. Huang, J. Han and S. Han, *Chemical Science*, 2012, **3**, 2941-2948.
30 F. Liu, Q. Zhao, H. You and Z. Wang, *Nanoscale*, 2013, **5**, 1047-1053.
31 A.-C. Faure, S. Dufort, V. Josserand, P. Perriat, J.-L. Coll, S. Roux and O. Tillement, *Small*, 2009, **5**, 2565-2575.
32 A.Avdeef, S. R.Sofen, T. L.Bregante, K. N.Raymond, *J. Am. Chem. Soc.* 1978, **100**, 5362-5370.
33 33.B. J. Kim, D. X. Oh, S. Kim, J. H. Seo, D. S. Hwang, A. Masic, D. K. Han and H. J. Cha, *Biomacromolecules*, 2014, **15**, 1579-1585.
34 B. P. Lee and S. Konst, *Advanced Materials*, 2014, **26**, 3415-3419.
35 G. H. Hwang, K. H. Min, H. J. Lee, H. Y. Nam, G. H. Choi, B. J. Kim, S. Y. Jeong and S. C. Lee, *Chemical Communications*, 2014, **50**, 4351-4353.
36 Y. Chen, Q. Yin, X. Ji, S. Zhang, H. Chen, Y. Zheng, Y. Sun, H. Qu, Z. Wang, Y. Li, X. Wang, K. Zhang, L. Zhang and J. Shi, *Biomaterials*, 2012, **33**, 7126-7137.
37 J. Liu, J. Bu, W. Bu, S. Zhang, L. Pan, W. Fan, F. Chen, L. Zhou, W. Peng, K. Zhao, J. Du and J. Shi, *Angewandte Chemie International Edition*, 2014, **53**, 4551-4555.
38 C. Kaittanis, T. M. Shaffer, A. Ogirala, S. Santra, J. M. Perez, G. Chiosis, Y. Li, L. Josephson and J. Grimm, *Nat Commun*, 2014, **5**, 3384-3394.
39 Y. Chen, D. Ye, M. Wu, H. Chen, L. Zhang, J. Shi and L. Wang, *Advanced Materials*, 2014, **26**, 7019-7026.
40 Y.-K. Peng, C.-L. Liu, H.-C. Chen, S.-W. Chou, W.-H. Tseng, Y.-J. Tseng, C.-C. Kang, J.-K. Hsiao and P.-T. Chou, *Journal of the American Chemical Society*, 2013, **135**, 18621-18628.
41 B. H. Kim, N. Lee, H. Kim, K. An, Y. I. Park, Y. Choi, K. Shin, Y. Lee, S. G. Kwon, H. B. Na, J.-G. Park, T.-Y. Ahn, Y.-W. Kim, W. K. Moon, S. H. Choi and T. Hyeon, *Journal of the American Chemical Society*, 2011, **133**, 12624-12631.
42 L. Cheng, C. Wang, L. Feng, K. Yang and Z. Liu, *Chemical Reviews*, 2014, **114**, 10869-10939.
43 R. W. Y. Habash, R. Bansal, D. Krewski and H. T. Alhafid, *Crit. Rev. Biomed. Eng.* 2006, **34**, 459-489.

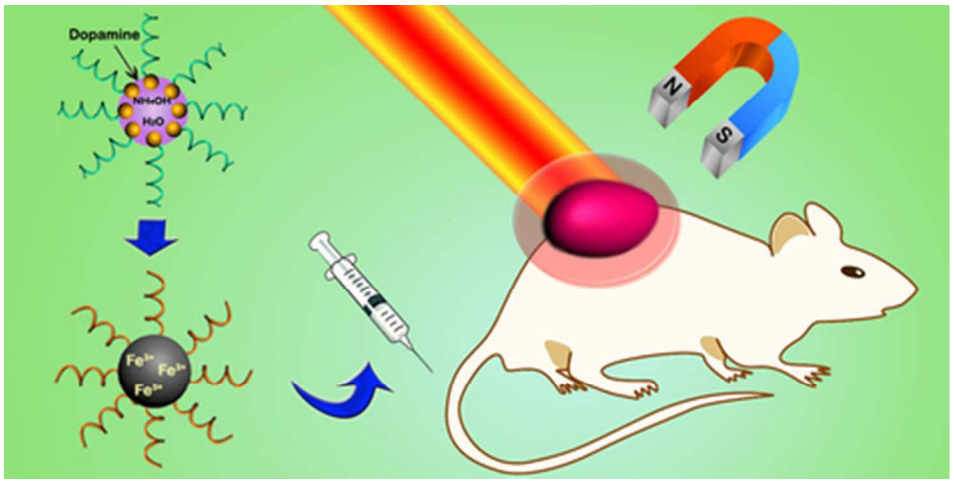

39x19mm (300 x 300 DPI)

A simple reverse microemulsion-based method was used to elaborate pH-activatable PEG-Fe-PDA nanoparticles for cancer diagnosis and therapy.